第 36 卷第 6 期 无 机 化 学 学 报 Vol.36 No.6
2020 年 6 月 CHINESE JOURNAL OF INORGANIC CHEMISTRY 1123-1130

氢键双螺旋双核化合物的介电和磁耦合性质

李 晶[1] 杨 莉[1] 尹 磊[2] 蒋尚达[3] 欧阳钟文[2] 张义权*[,4] 王振兴*[,2] 宋 友*[,1]
([1]南京大学化学化工学院,配位化学国家重点实验室,南京 210023)
([2]华中科技大学武汉国家高磁场中心,武汉 430074)
([3]北京大学化学与分子工程学院,国家分子科学实验室,
国家稀土材料化学与应用重点实验室,北京 100871)
([4]南京师范大学物理科学与技术学院,江苏省 NSLSCS 重点实验室,南京 210023)

摘要:制备了一个氢键桥联的双核 Co(Ⅱ)双螺旋化合物$[(L)CoCl]_2\cdot 2H_2O$(L=6-甲基吡啶-2-甲醇),并研究了它的介电和磁性质。磁性测试、HF-EPR 谱分析和介电性质均表明,该分子内氢键在磁交换相互作用和介电性能中起着重要作用,从头计算对这一结论给予进一步证明。

关键词:螺旋状双核 Co 配合物;氢桥键;介电;磁交换作用
中图分类号:O614.81+2 **文献标识码**:A **文章编号**:1001-4861(2020)06-1123-08
DOI:10.11862/CJIC.2020.117

Dielectric and Magnetic Exchange Natures of a Dinuclear Double-Stranded Hydrogen Bonds Helicates

LI Jing[1] YANG Li[1] YIN Lei[2] JIANG Shang-Da[3] OUYANG Zhong-Wen[2]
ZHANG Yi-Quan*[,4] WANG Zhen-Xing*[,2] SONG You*[,1]
([1]*State Key Laboratory of Coordination Chemistry, School of Chemistry and Chemical Engineering, Nanjing University, Nanjing* 210023, *China*)
([2]*Wuhan National High Magnetic Field Center, Huazhong University of Science and Technology, Wuhan* 430074, *China*)
([3]*National Laboratory for Molecular Sciences, State Key Laboratory of Rare Earth Materials Chemistry and Applications, College of Chemistry and Molecular Engineering, Peking University, Beijing* 100871, *China*)
([4]*Jiangsu Key Laboratory for NSLSCS, School of Physical Science and Technology, Nanjing Normal University, Nanjing* 210023, *China*)

Abstract: The dielectric and magnetic properties of a dinuclear Co(Ⅱ) double-stranded helicate containing hydrogen bridging bond have been investigated. Magnetic properties, HF-EPR spectra and dielectric properties all indicate that this intramolecular hydrogen bond plays an important role in the magnetic exchange interactions and dielectric properties. *Ab initio* calculations provide further support for above conclusions.

Keywords: dinuclear Co(Ⅱ) double-stranded helicate; hydrogen bridging bond; dielectric properties; magnetic exchange interaction

Among various supramolecular interactions, hydrogen bond can have different forms with variable strengths. It is regarded as a kind of electrostatic dipole-dipole interaction with some covalent bonding

收稿日期:2020-02-08。收修改稿日期:2020-03-18。
国家重点研发计划(No.2013CB922102,2017YFA0303200)和国家自然科学基金(No.21973038,21571097)资助项目。
*通信联系人。E-mail:yousong@nju.edu.cn,zxwang@hust.edu.cn,zhangyiquan@njnu.edu.cn

characters. It is responsible for the adhesion of molecules in liquids and thus very important in soft matter chemistry and biology. It is equally important in various inorganic and organic molecule systems[1]. Because of these special features, hydrogen bonds usually contribute to interesting physical properties and/or phenomenon in materials. In biology[2-3], hydrogen bond helps to build 3D proteins and double-helical DNA, and participates in most of bio-mechanism. In material science, hydrogen bond has been found to induce ferroelectric and dielectric properties[4-8]. Hydrogen bonds also play an important role in photo-induced proton/charge transfers[9-10], proton conduction[11-12] and self-healing materials[13]. Over the past decade, some magnetic clusters with hydrogen bonds have been reported, and they present cooperative magnetic properties compared to the isolated clusters[14-17]. However, the presence of three-dimensional hydrogen bond low-symmetry nets expands the complexity, such that the exchanges through the hydrogen bond in the systems are difficult to evaluate. In the magnetic clusters with hydrogen bonding, the proton provides an *s* orbital to mix with the orbitals of donor and acceptor atoms, so the clusters consist of a pathway to mediate magnetic coupling interaction between spin carriers (radical and metal ions)[14]. By taking this account of the hydrogen bond mediated interactions, many special magnetic properties might be explained smoothly. Furthermore, introduction of hydrogen bond in some systems can help tune/control spin-couplings or build magneto-electric coupling system, which might be promising potential applications in the spintronics. We found a reported Co(Ⅱ) dinuclear (**1**), $[(L)CoCl]_2 \cdot 2H_2O$ (L=6-methylpyridine-2-methanol), containing a pair of interesting intramolecular hydrogen bonds bridging between two spin moieties[18]. In this work, we investigated the magnetism and dielectricity in details combined with theoretical calculation and high-frequency EPR (HF-EPR), which shows that the hydrogen bonds play an important role on the properties. To the best of our knowledge, this is the first example that only hydrogen bonding mediated magnetic coupling is clearly illustrated.

1 Experimental

1.1 Synthesis of 1

All the chemical reagents were obtained commercially from J&K Scientific Ltd. without further purification. $CoCl_2 \cdot 6H_2O$ (83.9 mg), $Co(OAc)_2 \cdot 4H_2O$ (87.8 mg), and 6-methylpyridine-2-methanol (174 mg) were mixed in MeOH (1.5 mL) to give a dark red solution. Dioxane (2.5 mL) was then added to give a blue solution which was refrigerated for several days. The crystalline solid formed, and was filtered off and washed with cold MeOH. The CIF (CCDC: 219398) contains the supplementary crystallographic data for this paper[18]. Yield: 184 mg. Anal. Calcd. for $C_{28}H_{38}N_4O_6Co_2Cl_2$(%): C, 47.0; H, 5.35; N, 7.83. Found(%):C, 47.7; H, 5.41; N, 7.76. IR (KBr, cm^{-1}): 3 435 (m), 1 610 (s), 1 578 (m), 1 474 (s), 1 375 (m), 1 173 (m), 1 126 (m), 1 096 (m), 1 015 (s), 949 (s), 927 (m), 785 (m).

1.2 Physical measurements

The C, H, N microanalyses were carried out with a PE 2400 series Ⅱ elemental analyzer. The FT-IR spectra were recorded from KBr pellets in a range of 4 000~500 cm^{-1} on a PE spectrum one FT-IR spectrometer. Powder X-ray diffraction (PXRD) patterns were obtained at 293 K on a D8 ADVANCE (Cu $K\alpha_1$, λ= 0.154 056 nm; $K\alpha_2$, λ=0.154 439 nm) powered at 40 kV and 40 mA. The crystalline powder samples were prepared by crushing the crystals and the PXRD scanned from 5° to 50° at a rate of 5°·min^{-1}. Calculated PXRD patterns were generated using Mercury 3.9 (Fig.S1, Supporting information). Thermogravimetric analyses (TGA) were performed on a STA449F3 TG-DSC instrument in flowing N_2 at a heating rate of 5 ℃·min^{-1} in a range of 40~1 200 ℃. Dielectric permittivity measurements were performed on Broad Band Dielectric Spectrometer (Concept80). The diameter of sample for dielectric measurement was 6 mm and the thickness was 0.5 mm. The data of magnetic properties for crystalline samples were collected on a Quantum Design MPMS-XL 7 superconducting quantum interference device (SQUID) magnetometer. HF-EPR measurement was performed on a locally developed spectrometer at the Wuhan National High Magnetic

Field Centre, using a pulsed magnetic field of up to 10 T. The raw spectra obtained in an absorptive mode were subsequently digitally transformed into a derivative presentation.

2 Results and discussion

2.1 Structure description

Complex **1** was synthesized according to reference[18]. It crystallizes in the orthorhombic space group *Pbcn* (Fig.S1). The crystal structure of **1** consists of two trigonal bipyramid Co(Ⅱ) units bridged by a pair of hydrogen bonds through the pathway Co-O-H-O-Co. Two oxygen atoms of two ligands and a chloride ion construct the basal plane of the bipyramid with a mean deviation of 0.084 nm, while two nitrogen atoms of two ligands coordinate to Co(Ⅱ) ion by the axial direction. The alcohol hydroxyls of two units form the hydrogen bonds and bridge between two units forming a centre symmetrical dinuclear. The molecule is neutral and the separation of the two Co ions is 0.438 nm. The distance of the two oxygen atoms is 0.242 nm, which indicates a very strong hydrogen bond[19]. It is interesting to see both hydrogen atoms are biased toward one of two Co (Ⅱ) ions, showing that the molecule could be regarded as an inner salt (Table S1). With this rare structure feature, the complex should appear the magnetic properties different from mononuclear complex with the significant dielectric.

2.2 Dielectric property

The plots of real part of dielectric permittivity against temperature are depicted in Fig.1a, where the complex dielectric constant $\varepsilon^*=\varepsilon'-i\varepsilon''$, and ε' and ε'' are the real and imaginary parts of ε. With the frequency from low to high, the characteristic relaxation behavior of the dielectric permittivity could be observed for **1** in the temperature range of approximately 50 K. As increasing frequency, we could see that the step-like maximum of ε' shifted to higher temperatures, which can be a potential relaxation dielectric material[20-21]. The response temperature of ε'' was consistent with the real part of ε'. Moreover, when the frequency was in a range of 0.13 to 107 Hz, the dielectric constant increased more than twice from high to low temperature, which can be attributed to the polarization of hydrogen displacement. When we converted Fig.1a to the frequency dependence of dielectric permittivity, we could find that ε' quickly decreased and immediately reached a platform area (Fig.1b). As the frequency continued to increase, the ε' droped once again and showed the second platform above 104 Hz. The first decrease of ε' in low frequency should be from the space charge possibly based on the defect and surface of crystals. The observed platform is ascribed to the inherent dipole of molecules. Above 104 Hz the dielectric permittivity was slightly lower than 10, indicating the existence of ionic displacement polarization within dinuclear molecule.

The imaginary part ε'' as a function of alternating-current (ac) frequency exhibited a broad peak in 0.01 to 1 000 Hz just where the ε' droped most steeply. This behaviour is characteristic of a

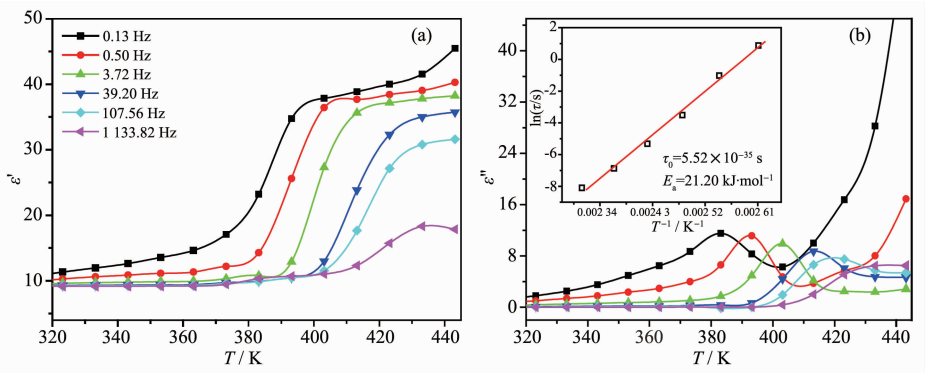

Inset: Arrhenius plots of $\ln\tau$ vs T^{-1}; red lines show the fit of data to Arrhenius expression $\tau=\tau_0\exp[E_a/(k_BT)]$

Fig.1　Temperature dependence of real ε' and ε'' part of dielectric permittivity for **1**

Debye-like dielectric relaxation, in which the reorientation of dipoles cannot respond to the applied ac electric field when high frequency exceeds a relaxation rate $1/\tau$ (where τ is the relaxation time) and it can be expressed as Eq.(**1**):

$$\varepsilon^{*}=\varepsilon_{\infty}+\frac{\varepsilon_{s}-\varepsilon_{\infty}}{1+(i\omega\tau)^{a}}$$

$$\varepsilon'=\varepsilon_{\infty}+\frac{(\varepsilon_{s}-\varepsilon_{\infty})[1+\cos(\frac{\alpha\pi}{2}\omega^{a}\tau^{a})]}{1+2\cos(\frac{\alpha\pi}{2}\omega^{a}\tau^{a})+\omega^{2a}\tau^{2a}}$$

$$\varepsilon''=\frac{(\varepsilon_{s}-\varepsilon_{\infty})\sin(\frac{\alpha\pi}{2}\omega^{a}\tau^{a})}{1+2\cos(\frac{\alpha\pi}{2}\omega^{a}\tau^{a})+\omega^{2a}\tau^{2a}} \quad (\mathbf{1})$$

The temperature dependence of resulted relaxation times were fitted to the Arrhenius law of $\tau=\tau_0\exp[E_a/(k_BT)]$, and the activity energy E_a and relaxation time τ_0 were calculated to be 21.20 kJ·mol^{-1}, 5.52×10^{-35} s (Fig.1, Inset). The relaxing mechanisms can be justified by the information of ε'' data (Fig.1) and the relaxing process is consistent with characteristic behaviour of the dielectric permittivity in Fig.S4, which is different from the relaxation dielectric behaviours of ferroelectric compounds[22]. To explain the relaxation dielectric properties of **1**, the dipolar moment of different hydrogen displacements were calculated by changing the O3-H1 bond length (Fig.2). When the H atoms were closer to the O3, the dipolar moment of the dimer complex was larger. As a result, when the crystals were placed in an electric field, the dielectric permittivity was changed due to the H^+ displacement driven by the electrostatic force and thermal disturbance.

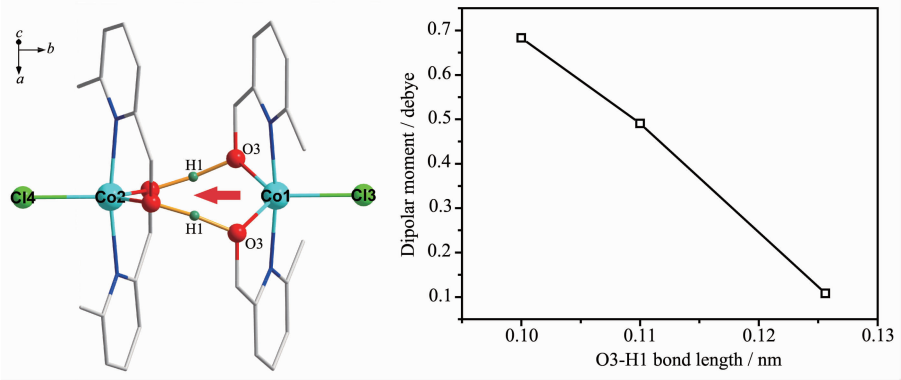

Red arrow in the left picture reprents the direction of the dipolar moment

Fig.2 Relationship between dipolar moment and the length of O3-H1 bond based on *ab initio* calculations

2.3 Magnetic properties

The direct-current (dc) magnetic measurements were performed on polycrystalline powder of **1** under 1.0 kOe in a temperature range of 1.8~300 K (Fig.3a). The χ_MT product at room temperature was 4.78 cm^3·mol^{-1}·K, which was larger than the expected 3.75 cm^3·mol^{-1}·K for two isolated Co(Ⅱ) ions, owing to the strong spin-orbital coupling of Co(Ⅱ)[23]. As the temperature was lowered, the χ_MT product stayed almost a constant above 150 K, then decreased continuously down to 0.3 cm^3·mol^{-1}·K at 1.8 K, suggesting to be due to intrinsic magnetic anisotropy of the Co(Ⅱ) ions and antiferromagnetic interaction between the metal ions[23]. The plot of χ_M versus T revealed a peak at 5 K, which is the typical feature of short-range antiferromagnetic ordering between spins. Namely, the antiferromagnetic coupling interaction between Co(Ⅱ) ions mediated by hydrogen bonding is strong enough and leads to the antiparallel arrangement of the spins of two Co(Ⅱ) ions below 5 K. Isothermal field-dependence magnetization was measured at low temperature from 0 to 70 kOe. The curves revealed S-shaped profiles at 1.8 and 3 K due to the decoupling of magnetic field, which gives the further evidence for the antiferromagnetic interaction within the dimer Co(Ⅱ) ions. The magnetization at 6 K is larger than the ones at 1.8 and 3 K below 2 T in good correlation with a weak antiferromagnetic exchange interaction (Fig.S6).

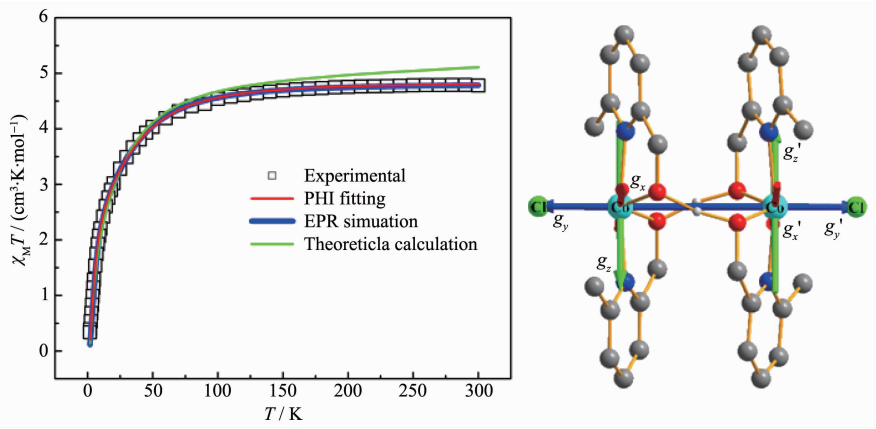

Red lines are the fitting results with PHI program, Green line is from CASPT2/RASSI calculations and the blue line is calculated with the parameters from the EPR simulation

Fig.3　(a) Magnetic susceptibility of complex **1** under 1.0 kOe dc field in a temperature range of 1.8~300 K; (b) Orientations of the local magnetic axes for the ground doublet on Co(Ⅱ) ions of complex **1**

Complex **1** has been in the fully paramagnetic phase above 6 K because the temperature effect has overwhelmed the coupling interaction between Co(Ⅱ) ions. The experimental $\chi_M T$ data and magnetizations were fitted concurrently using the PHI program with the following spin Hamiltonian[24]:

$$\hat{H}=-2J\hat{S}_1\hat{S}_2+\sum\{D[\hat{S}_{iz}{}^2-S_i(S_i+1)/3]+E(\hat{S}_{ix}{}^2-\hat{S}_{iy}{}^2)+\mu_B gB\hat{S}_i\} \quad (2)$$

The best fitting result is summarized in Table 1. The zero-field splitting parameter $D>0$, indicating the trigonal bipyramid Co(Ⅱ) exhibits easy-plane anisotropy. The interaction within the Co(Ⅱ) dimer through the bridging hydrogen bond is weak antiferromagnetic. In contrast to slow magnetic relaxation behaviour reported by Dunbar et al.[25] and Mallah et al.[26] for a serial of trigonal bipyramid Co(Ⅱ) complexes, no out-of-phase magnetic susceptibility signal was observed for **1**, in 0 or 4.0 kOe external bias dc field (Fig.S7). Importantly, this is consistent with that the antiferromagnetic interaction between the symmetrically placed Co(Ⅱ) moments through hydrogen bond would stabilize an $S_T=0$ ground state and thus no single molecule magnetism is expected[27].

To further investigate the magnetic coupling of this complex, theoretical calculations were performed using Complete Active Space Second-order Multiconfigurational Perturbation Theory (CASPT2) and considering the effect of the dynamic electron correlation based on complete-active-space self-consistent field (CASSCF) method within the MOLCAS 8.0 program package[28] on individual Co(Ⅱ) fragment. The exchange interaction in complex **1** was estimated by BS-DFT (B3LYP[29-30] method combined with broken symmetry approach) calculations and Lines model[31] based on CASPT2 results, respectively. The energy difference

Table 1　Detailed parameters from the PHI fitting, theoretical calculation and EPR simulations

		PHI fitting		Calculation		EPR simulation
		iso	aniso	BS-DFT	CASPT2	aniso
g	g_x	2.284	2.298	2.430		2.38
	g_y		2.399	2.339		2.35
	g_z		2.100	2.020		2.05
J / cm^{-1}		−0.77	−0.86	−1.14	−1.10	−1.15
D / cm^{-1}		35.7	42.448	—	37.5	42.448
E / cm^{-1}		−10.77	−11.76	—	−3.80	−2.7
zJ' / cm^{-1}		−0.005	0.0441	—	−0.08	0

between the lowest two spin-free states for complex **1** was found to be much larger than that between the lowest two spin-orbit states (Table S2 and S3). Thus, the ZFS parameters D and E to depict their magnetic anisotropies are reasonable. The calculated D, E (cm^{-1}) and g tensor (x, y, z) for **1** are listed in Table 1, where the calculated D value is positive. The calculated orientations of the g_x, g_y, and g_z (hard axis) on Co(Ⅱ) are shown in Fig.3b. The calculated temperature dependence of $\chi_M T$ is shown in Fig.3 (left), where the fit is close to the experimental data especially in the low temperature range. From Table 1, the calculated isotropic Co(Ⅱ)-Co(Ⅱ) coupling constants using BS-DFT and Lines model based on CASPT2 results are almost the same, and the negative J value confirms that the Co(Ⅱ)-Co(Ⅱ) coupling is antiferromagnetic. To extract the contribution of the magnetic exchange interaction through the hydrogen bond, the isotropic coupling constants were separated into two parts of dipole-dipole and magnetic exchange interactions. The J dipolar is much small, and can be neglected (J_x=−0.03 cm^{-1}; J_y=0.06 cm^{-1}; J_z=−0.02 cm^{-1}, compared to J=−1.1 cm^{-1}). The antiferromagnetic exchange interaction through the hydrogen-bond is dominated. As a result, the hydrogen bond is the main factor for tuning the magnetism of the trigonal bipyramid [$Co^{Ⅱ}_2$].

2.4 HF-EPR measurements

HF-EPR measurements were carried out on powder samples of **1** for helping to understand the magnetic phenomenon. Fig.4a shows the variable-temperature (2~20 K) spectra collected at 170 GHz. The strength of peaks 1, 2, 5 increased with temperature, indicating population of excited states in the temperature range. Peaks 3, 4, 6 correspond to the ground state. The peaks 3, 4, 6 were observed at 2 K, indicating the resonance signals are from the single Co (Ⅱ) ions other than the dimer with S_T =0. The coexistence of ground and excited states indicates the existence of the magnetic coupling between the dimer Co(Ⅱ) unit[32], which is in line with the magnetic prop-

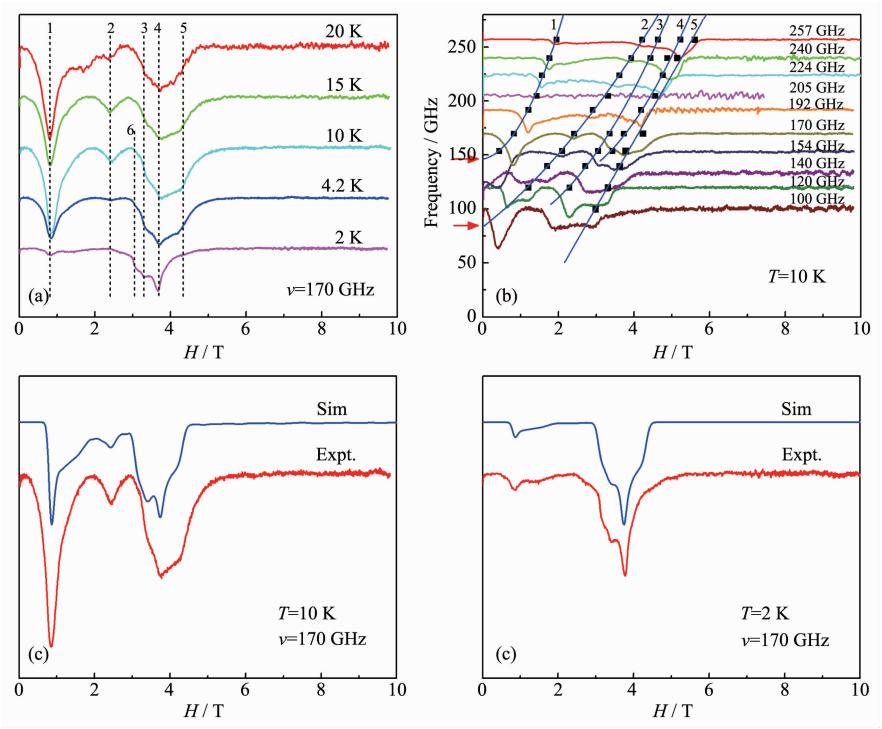

Fig.4 (a) HF-EPR spectra of **1** at different temperatures and 170 GHz; (b) HF-EPR spectra of **1** at 10 K and various frequencies, the spectra are offset in proportion to the frequency, black dots represent the resonance fields for each spectrum, solid lines 1~4 are the 2nd order polynomial fit to each resonance branch, solid line 5 is the linear fit to the resonance branch, red arrows indicate the energy gaps; (c, d) Experimental and simulated HF-EPR spectra of **1** at the frequency of 170 GHz and the temperature of 10 and 2 K, respectively

erties measurements. The right panel of Fig.4b shows the variable-frequency spectra collected at 10 K for **1**. Tracing the resonance field at various frequencies results in some energy gaps (zero-field splitting) with the amplitudes of several cm^{-1} for a specific spin state. Equation (**1**) was also employed to simulate the EPR spectra with the assumption that the principal axes of the local D and g tensors of the two Co(Ⅱ) ions coincide (Fig.3b). It was found in the attempts that the EPR spectra were not sensitive to the amplitude of D rather were very sensitive to J and E, so the value of D (42.448 cm^{-1}) from the PHI fitting was fixed and J and g values were allowed to vary. As shown in Fig.3c and 3d, the EPR spectra were well simulated, and the used parameters were presented in Table 1. The EPR simulations support the antiferromagnetic interaction between the Co(Ⅱ) ions as predicted by the susceptibility measurements and theoretical calculations above. With the spin parameters obtained from HF-EPR, we were able to reproduce the magnetic susceptibility data in the whole temperature range, confirming the validity of the obtained parameter values from HF-EPR (the blue line in Fig.3).

3 Conclusions

In conclusion, the foregoing results suggest that hydrogen-bonds involved in the bridge within the Co(Ⅱ) dimer provide moderate magnetic exchange interaction. The s orbital of proton in Co–O···H···O–Co provides a channel for the antiferromagnetic exchange interaction, leading to a total spin ground state S_T of zero at very low temperatures. Thus, the dimer does not present the SMM behavior. As the hydrogen displacement with the electric field, the complex exhibits obvious dielectric property at high temperature. In complex **1**, the intramolecular hydrogen bond strength is much weaker than the covalent bond, which can be tuned by the magnet field due to the antiferromagnetic interaction/Dzyaloshinskii-Moriya interaction between two Co(Ⅱ) ions. It would be a good chance to achieve the magneto-electric coupling[33-35]. Hydrogen bonds provide a new strategy to tune/control spin and electric field, even build the magneto-electric coupling system, which might have a promising application in spintronics.

Supporting information is available at http://www.wjhxxb.cn

References:

[1] Arunan E, Gautam R D, Roger K A, et al. *Pure Appl. Chem.*, **2011**,**83**:1619-1636

[2] Regina P, Daniel H. *Chem. Commun.*, **2010**,**46**:6449-6451

[3] Hellgren M, Kaiser C, de Haij S, et al. *Cell. Mol. Life Sci.*, **2007**,**64**:3129-3138

[4] Tayi A S, Kaeser A, Matsumoto M, et al. *Nat. Chem.*, **2015**, **7**:281-294

[5] Horiuchi S, Tokunaga Y, Giovannetti G, et al. *Nature*, **2010**, **463**:789-792

[6] Horiuchi S, Kobayashi K, Kumai R, et al. *Nat. Commun.*, **2017**,**8**:14426-14436

[7] Maczka M, Gagor A, Ptak M, et al. *Chem. Mater.*, **2017**,**29**: 2264-2275

[8] Sieradzki A, Pawlus S, Tripathy S N, et al. *Dalton Trans.*, **2017**,**46**:3681-3687

[9] Schier S H. *J. Am. Chem. Soc.*, **2015**,**137**:8860-8871

[10]Glover S D, Parada G A, Markle T F, et al. *J. Am. Chem. Soc.*, **2017**,**139**:2090-2101

[11]Ramaswamy P, Wong N E, Shimizu G K H. *Chem. Soc. Rev.*, **2014**,**43**:5913-5932

[12]Kang D W, Lim K S, Lee K J, et al. *Angew. Chem. Int. Ed.*, **2016**,**55**:16123-16126

[13]Oh J Y, Gagné S R, Chiu Y C, et al. *Nature*, **2016**,**539**:411-415

[14]Maspoch D, Catala L, Gerbier P, et al. *Chem. Eur. J.*, **2002**, **8**:3635-3645

[15]Cortijo M, Prieto R G, Herrero S, et al. *Eur. J. Inorg. Chem.*, **2013**,**32**:5523-5527

[16]Pinkowicz D, Southerland H I, Avendano C, et al. *J. Am. Chem. Soc.*, **2015**,**137**:14406-14422

[17]Wernsdorfer W, Aliaga-Alcalde N, Hendrickson D N, et al. *Nature*, **2002**,**416**:406-409

[18]Telfer S G, Sato T, Kuroda R. *Angew. Chem. Int. Ed.*, **2004**, **43**:581-584

[19]Emsley J. *Chem. Soc. Rev.*, **1980**,**9**:91-124

[20]Homes C C, Vogt T, Shapiro S M, et al. *Science*, **2001**,**293**: 673-676

[21]Zhang H Y, Hu C L, Hu Z B, et al. *J. Am. Chem. Soc.*, **2020**,**142**:3240-3245

[22]Zhang W, Xiong R G. *Chem. Rev.*, **2012**,**112**:1163-1195

[23]Kahn O. *Molecular Magnetism*. New York: John Wiley & Sons, **1993**.

[24]Chilton N F, Anderson R P, Turner L D, et al. *J. Comput. Chem.*, **2013**,**34**:1164-1175

[25]Woods T J, Rivas M F B, Coca S G, et al. *J. Am. Chem. Soc.*, **2016**,**138**:16407-16416

[26]Shao F, Cahier B, Riviere E, et al. *Inorg. Chem.*, **2017**,**56**:1104-1111

[27]Hu Z B, Feng X, Li J, et al. *Dalton Trans.*, **2020**,**49**:2159-2167

[28]Karlström G, Lindh R, Malmqvist P, et al. *Comput. Mater. Sci.*, **2003**,**28**:222-239

[29]Becke A D. *J. Chem. Phys.*, **1993**,**98**:5648-5652

[30]Becke A D. *Phys. Rev. A*, **1988**,**38**:3098-3100

[31]Lines M E. *J. Chem. Phys.*, **1971**,**55**:2977-2984

[32]Abragam A, Bleaney B. *Electron Paramagnetic Resonance of Transition Ions*. U.K.: Oxford University Press, **2012**.

[33]Yang L, Li J, Pu T C, et al. *RSC Adv.*, **2017**,**7**:47913-47919

[34]Chen L H, Guo J B, Wang X, et al. *Adv. Mater.*, **2017**,**29**:1702512

[35]Long J, Ivanov M S, Khomchenko V A, et al. *Science*, **2020**, **367**:671-676